Supplement of Atmos. Chem. Phys., 19, 3821–3831, 2019
https://doi.org/10.5194/acp-19-3821-2019-supplement

Atmospheric Chemistry and Physics
Open Access
EGU

Supplement of

Urban source term estimation for mercury using a boundary-layer budget method

Basil Denzler et al.

Correspondence to: Christian Bogdal (christian.bogdal@chem.ethz.ch)

Boundary-layer investigation

Advanced model set-up

An advanced scenario is designed to focus on the variability of the boundary-layer heights. The goal is to investigate how the basic scenario performs, regarding its assumption of constant NBL and CBL height, in comparison to an advanced scenario with a more lifelike representation of the boundary-layer heights. To accomplish this, we use the data of the COSMO-2 model, a numerical weather model with 2.2 km by 2.2 km resolution from MeteoSchweiz (Swiss Federal Office of Meteorology and Climatology). The heights are obtained by using the bulk Richardson number (Ri_b) as a stability criteria. Ri_b is built by the ratio of production or dissipation of turbulence by buoyancy and the mechanical turbulence through wind shear. It is a widely used stability criteria in numerical weather prediction models (Richardson et al., 2013). A critical threshold value for Ri_b of 0.33 Wetzel (1982) for calculating the height of the NBL and 0.22 (Vogelezang and Holtslag, 1996) for CBL is used. If the Ri_b approach misses to provide a boundary-layer height, it is determined by the vertical gradient of the potential temperature with a critical value of $<$0.72 K/100 m according to Szintai and Kaufmann (2008).

Advanced scenario

The comparison of the BLH modeled in the two scenarios – e.g. the basic scenario with constant BLH and the advanced scenario with the BLH derived from meteorological models – shows two main differences in Figure 3a. Firstly, the BLH during the day rises higher for the advanced scenario. This, however, does not have a strong influence on the modeled concentration since in both cases modeled concentration do approach background concentrations during the day (Fig. 3d). The second difference concerns the nighttime BLH, which for the advanced scenario forms earlier in the evening and is not as stable. Its height differs between the nights and is often larger than 150 m, especially towards the end of the selected period. This leads to modeled concentrations which do not reach the same levels as the measurements. At times, modeled concentrations for the basic run decline faster than the measurements in the morning. This suggests the transition of the BLH from nocturnal to daytime to be smoother than the step function in the basic scenario. The advanced scenario better accounts for that. With 5.7 g/hour the emission estimate for the advanced method is slightly higher than for the basic scenario during the selected period. In average over all periods, however, with 5.2 g/hour GEM emissions for the advanced scenario are slightly lower than for the basic run. For some periods selected for the characteristic day/night pattern, the estimation of the BLH do not follow the expected trends and no clear day/night inversion is observable. These periods are highlighted in gray in Table S1 and are not included in the evaluation for the advanced method. Considering the additional complexity and the additional data requirements of the advanced method, we clearly favor the basic method to assess the cities source strength. But we can use the alternative estimation of the BLH conducted for this scenario as a valuable validation. The proximity of the two methods regarding the emission estimates supports the way the BLH is set for the basic scenario.

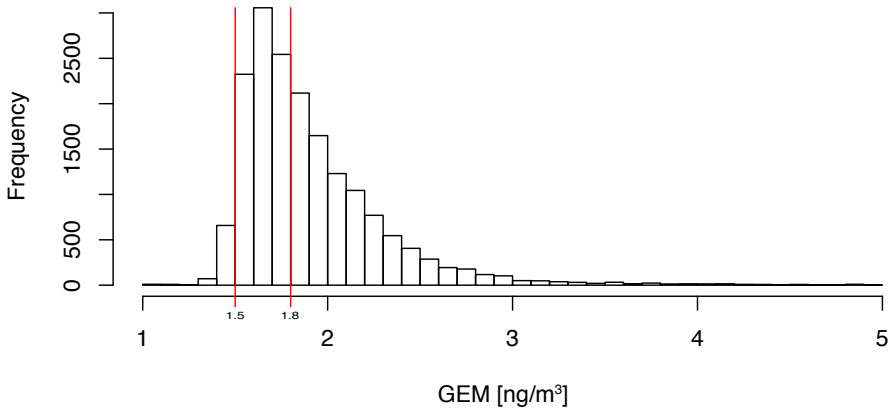

Figure S1. Histogram of GEM concentrations in Zurich from December 2013 until December 2015. Red lines show background levels as they were chosen for the box model.

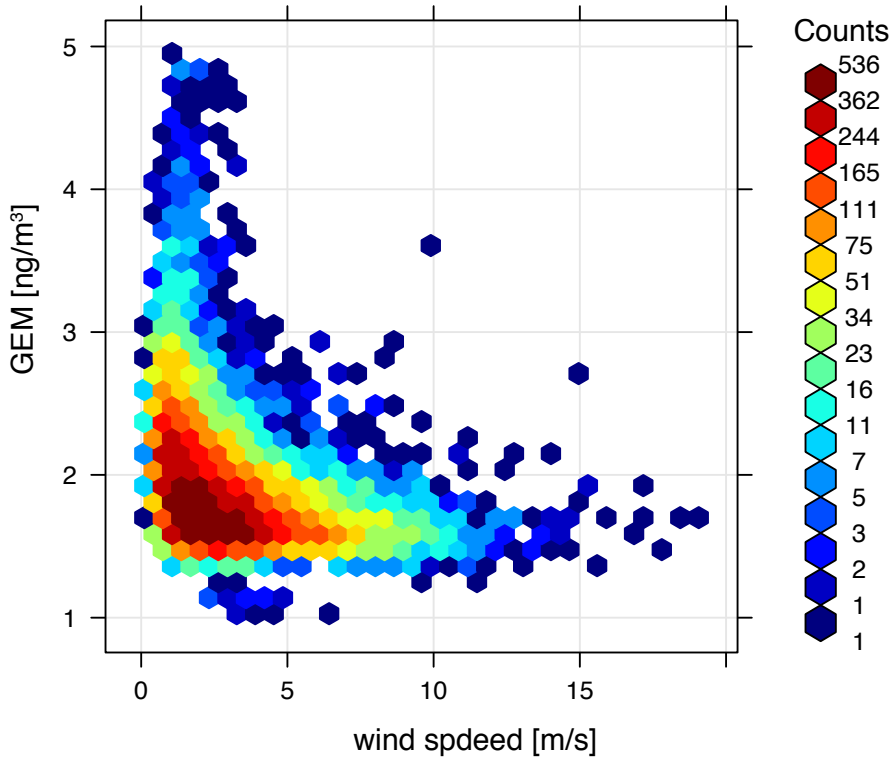

Figure S2. Scatter plot for GEM concentrations and wind speed in Zurich. The tiles represent the number of incidences.

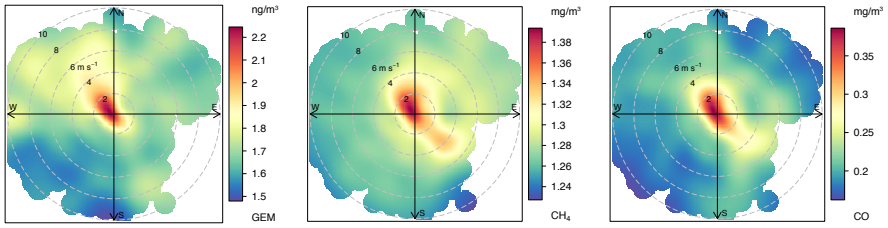

Figure S3. Wind rose plots for GEM, CH_4 and CO concentrations measured in Zurich over the course of 2 years, from December 2013 until December 2015.

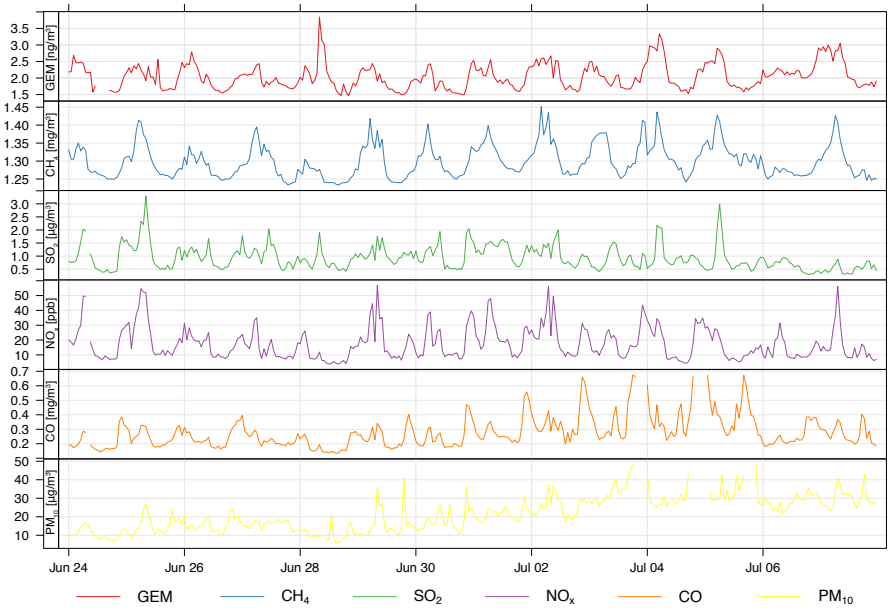

Figure S4. Pollutant measurements for a summer inversion period in Zurich from 24.06.2015 until 7.07.2015.

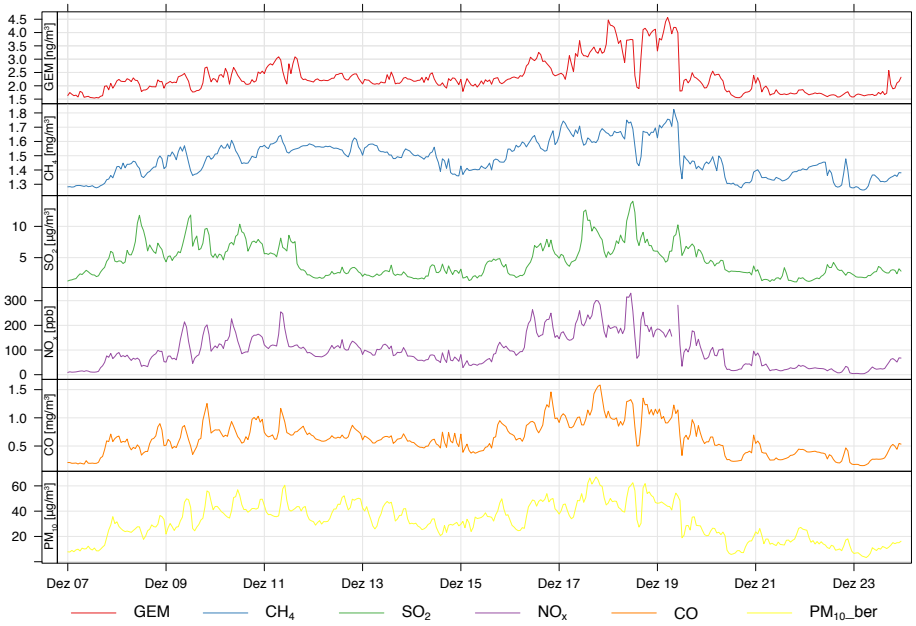

Figure S5. Pollutant measurements for a winter inversion period in Zurich from 07.12.2013 until 24.12..2013.

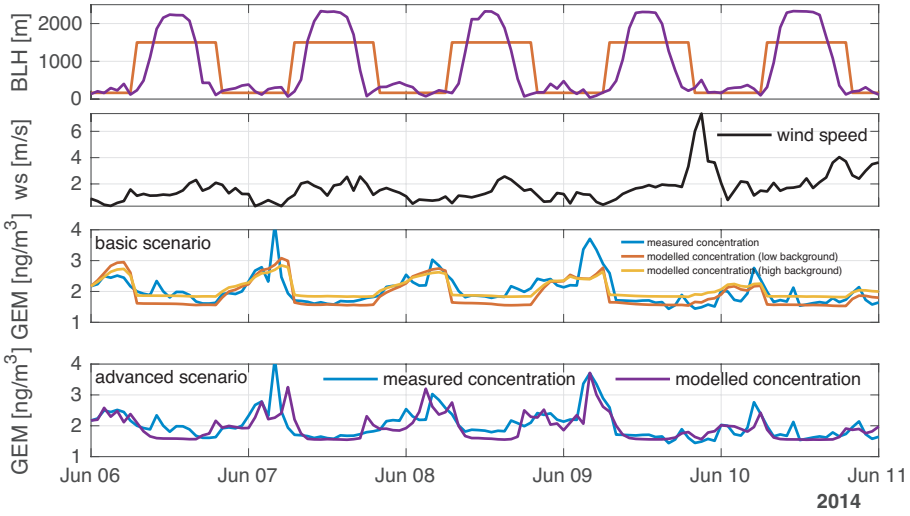

Figure S6. Period with day-night inversion showing the boundary layer height, as approximated in the model; basic scenario (red), advanced scenario (purple). The wind speed (black) is shown in he second plot. The third shows the diurnal pattern for GEM measurements (blue) with the basic scenario model results for high (yellow) and low background (red). The last plot shows the output of the advanced scenario (purple).

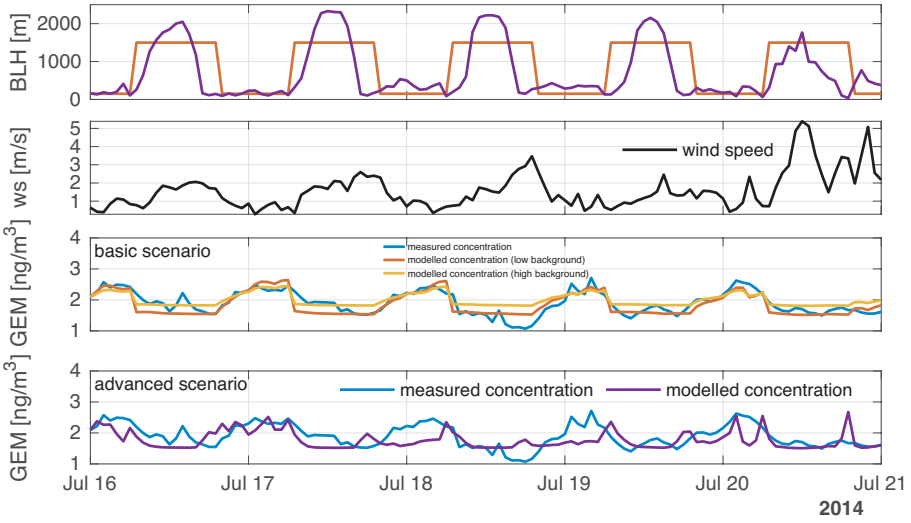

Figure S7. Period with day-night inversion showing the boundary layer height, as approximated in the model; basic scenario (red), advanced scenario (purple). The wind speed (black) is shown in he second plot. The third shows the diurnal pattern for GEM measurements (blue) with the basic scenario model results for high (yellow) and low background (red). The last plot shows the output of the advanced scenario (purple).

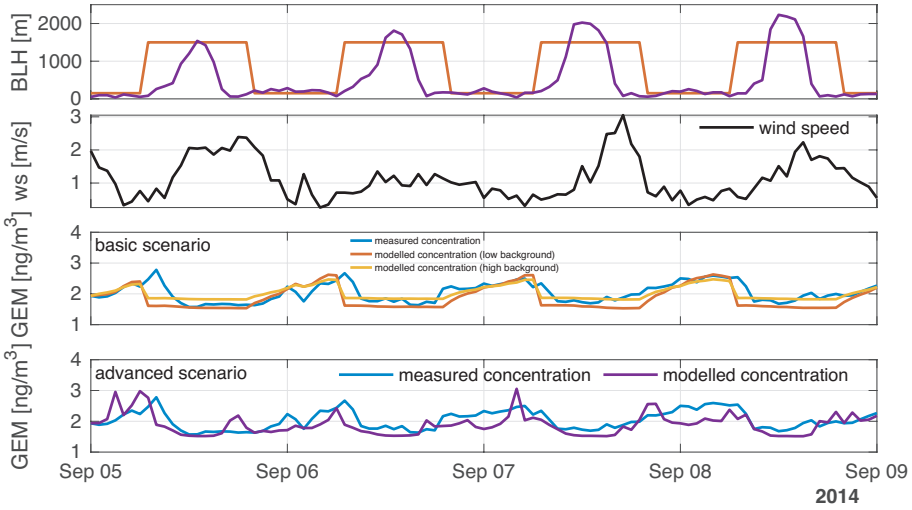

Figure S8. Period with day-night inversion showing the boundary layer height, as approximated in the model; basic scenario (red), advanced scenario (purple). The wind speed (black) is shown in he second plot. The third shows the diurnal pattern for GEM measurements (blue) with the basic scenario model results for high (yellow) and low background (red). The last plot shows the output of the advanced scenario (purple).

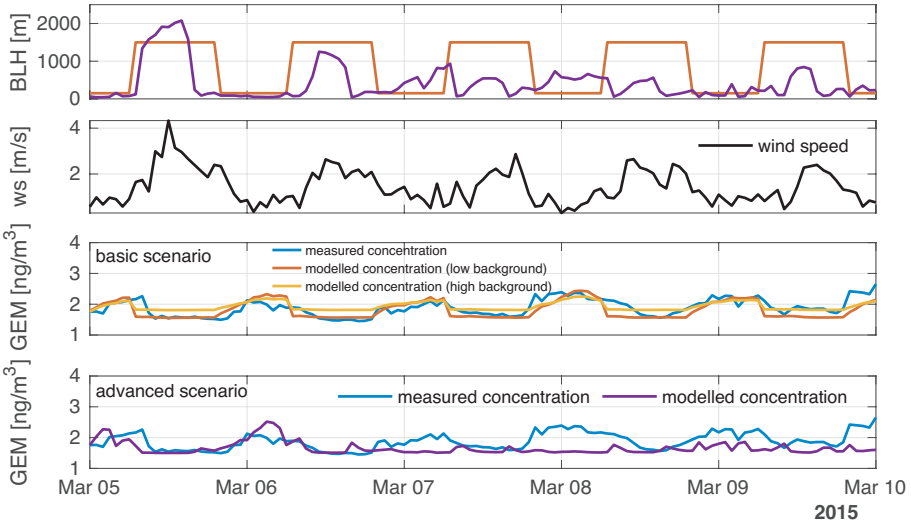

Figure S9. Period with day-night inversion showing the boundary layer height, as approximated in the model; basic scenario (red), advanced scenario (purple). The wind speed (black) is shown in he second plot. The third shows the diurnal pattern for GEM measurements (blue) with the basic scenario model results for high (yellow) and low background (red). The last plot shows the output of the advanced scenario (purple).

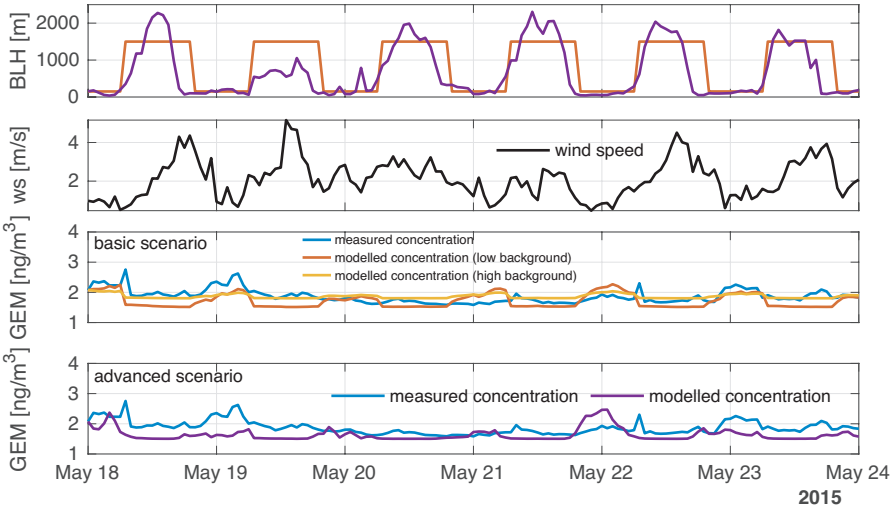

Figure S10. Period with day-night inversion showing the boundary layer height, as approximated in the model; basic scenario (red), advanced scenario (purple). The wind speed (black) is shown in he second plot. The third shows the diurnal pattern for GEM measurements (blue) with the basic scenario model results for high (yellow) and low background (red). The last plot shows the output of the advanced scenario (purple).

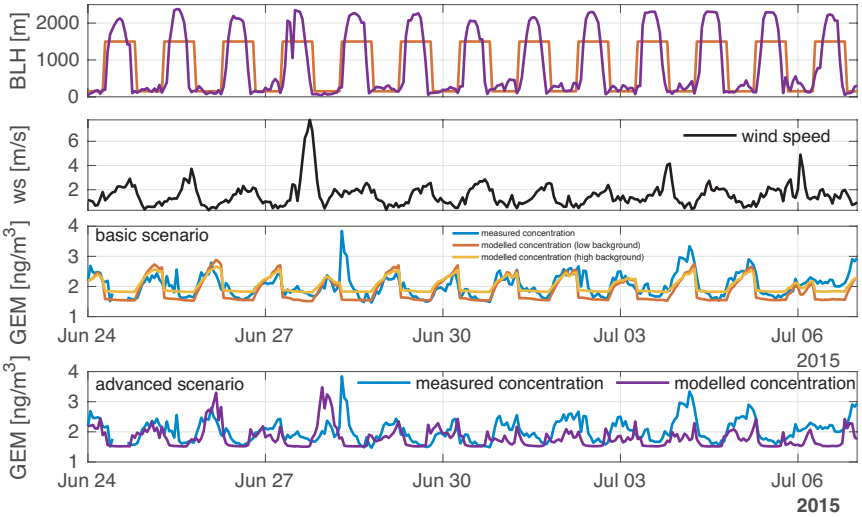

Figure S11. Period with day-night inversion showing the boundary layer height, as approximated in the model; basic scenario (red), advanced scenario (purple). The wind speed (black) is shown in he second plot. The third shows the diurnal pattern for GEM measurements (blue) with the basic scenario model results for high (yellow) and low background (red). The last plot shows the output of the advanced scenario (purple).

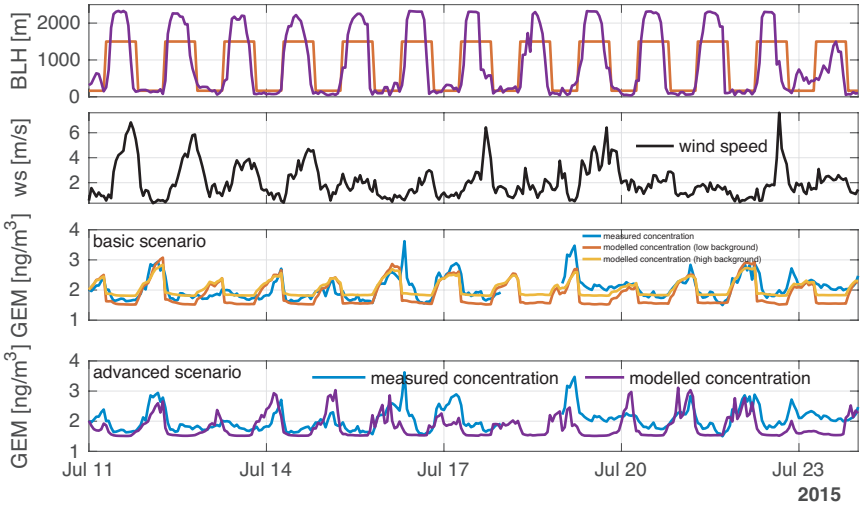

Figure S12. Period with day-night inversion showing the boundary layer height, as approximated in the model; basic scenario (red), advanced scenario (purple). The wind speed (black) is shown in he second plot. The third shows the diurnal pattern for GEM measurements (blue) with the basic scenario model results for high (yellow) and low background (red). The last plot shows the output of the advanced scenario (purple).

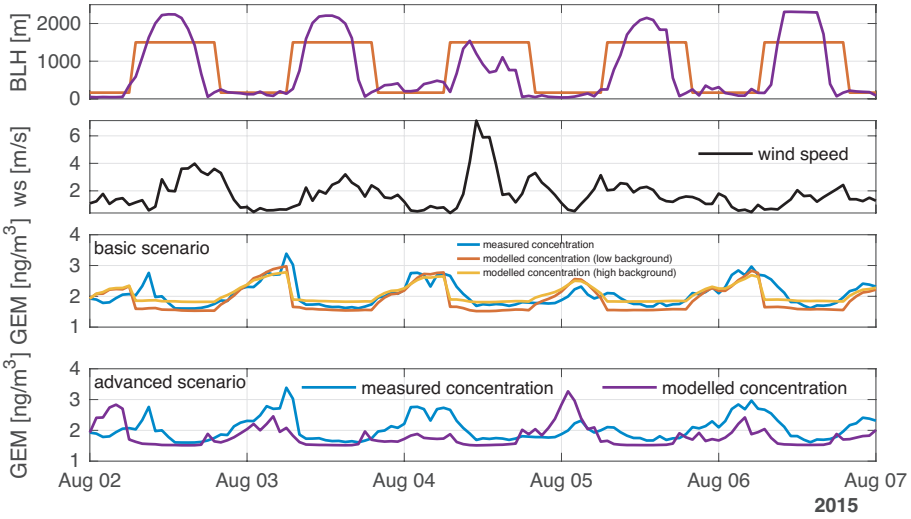

Figure S13. Period with day-night inversion showing the boundary layer height, as approximated in the model; basic scenario (red), advanced scenario (purple). The wind speed (black) is shown in he second plot. The third shows the diurnal pattern for GEM measurements (blue) with the basic scenario model results for high (yellow) and low background (red). The last plot shows the output of the advanced scenario (purple).

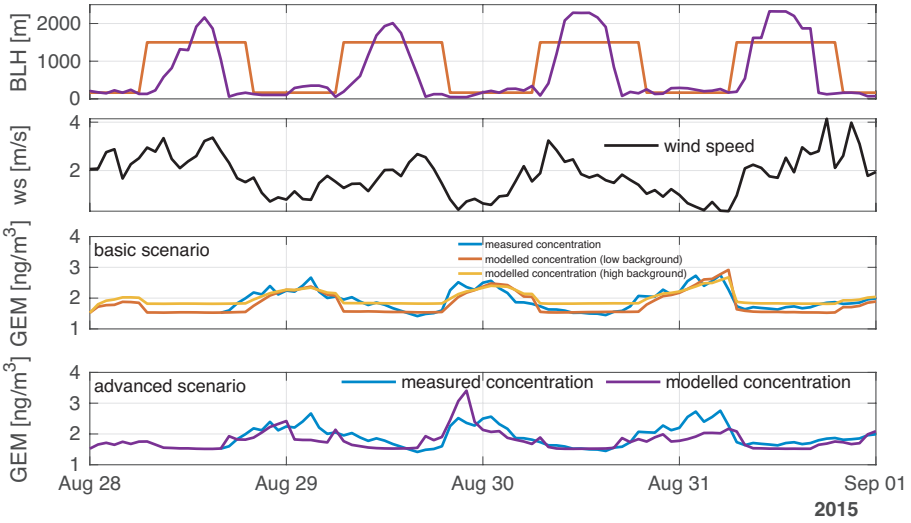

Figure S14. Period with day-night inversion showing the boundary layer height, as approximated in the model; basic scenario (red), advanced scenario (purple). The wind speed (black) is shown in he second plot. The third shows the diurnal pattern for GEM measurements (blue) with the basic scenario model results for high (yellow) and low background (red). The last plot shows the output of the advanced scenario (purple).

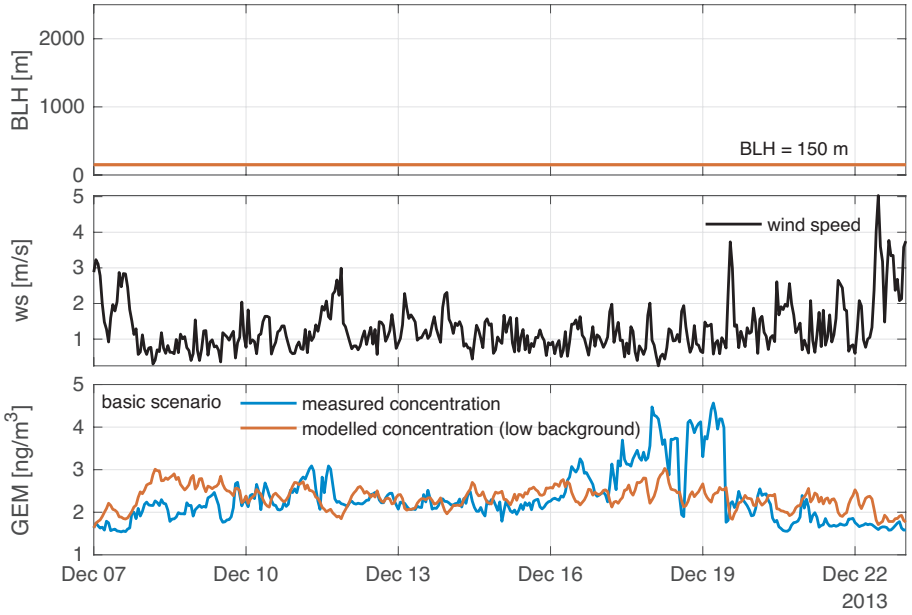

Figure S15. Winter period with stable inversion showing the boundary layer height, as approximated in the model; basic scenario (red), 150 m. The wind speed (black) is shown in he second plot. The third shows the diurnal pattern for GEM measurements (blue) with the basic scenario model results (red).

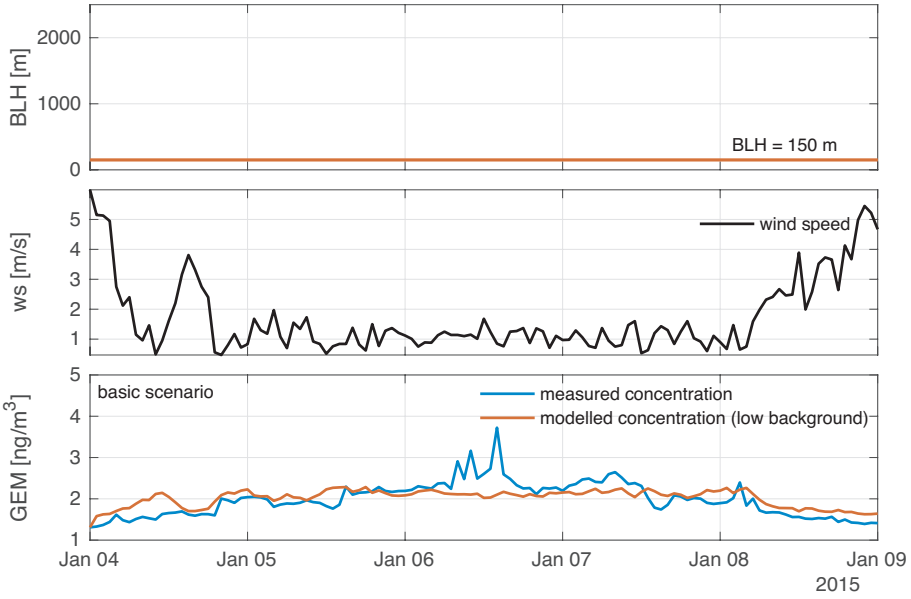

Figure S16. Winter period with stable inversion showing the boundary layer height, as approximated in the model; basic scenario (red), 150 m. The wind speed (black) is shown in he second plot. The third shows the diurnal pattern for GEM measurements (blue) with the basic scenario model results (red).

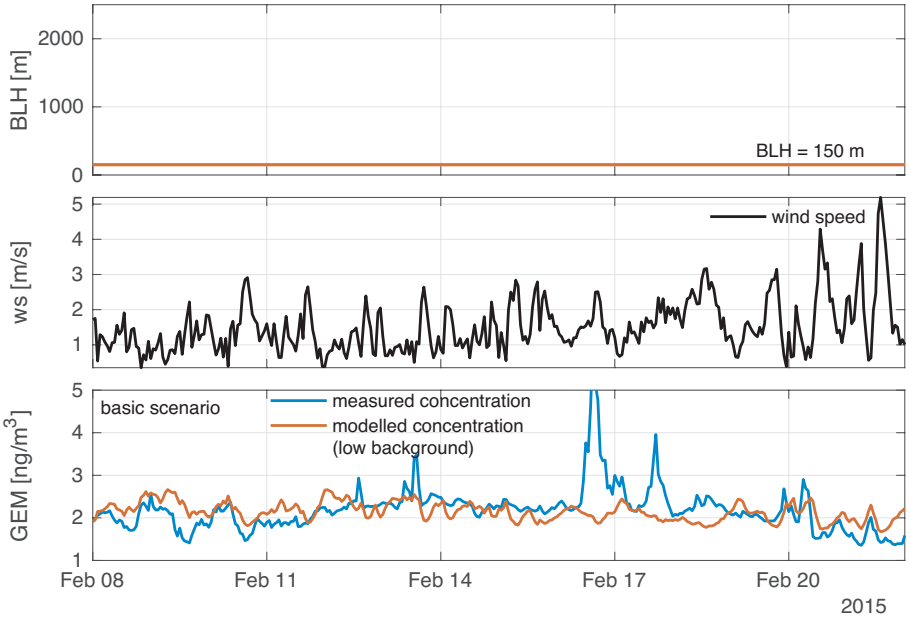

Figure S17. Winter period with stable inversion showing the boundary layer height, as approximated in the model; basic scenario (red), 150 m. The wind speed (black) is shown in he second plot. The third shows the diurnal pattern for GEM measurements (blue) with the basic scenario model results (red).

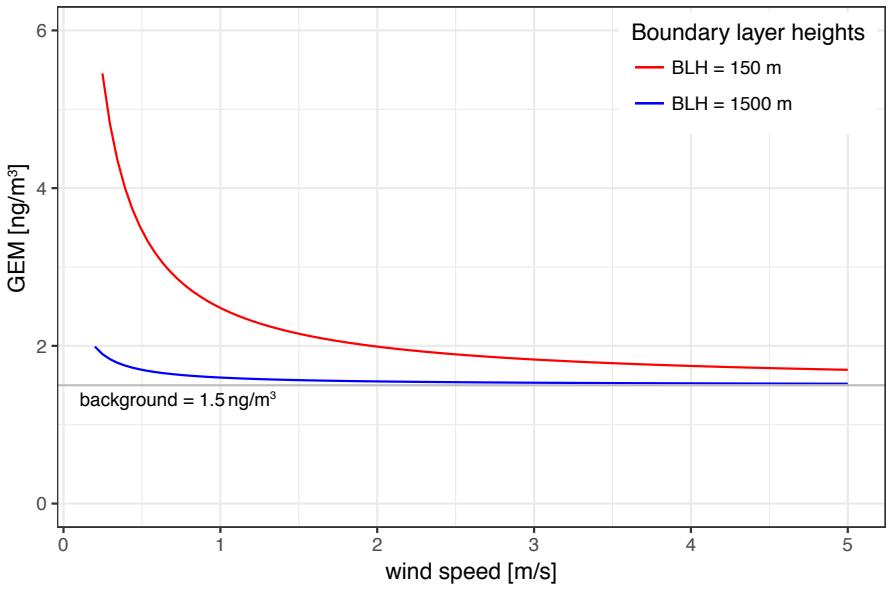

Figure S18. For the steady state assumption $c = c_{\text{back}} + E/(u \cdot A_{\text{s}})$, GEM concentrations are displayed for the lower air compartment depending on the wind speed once for a boundary layer height of 150 m (red) and for a height of 1500 m (blue). Background concentrations are 1.5 ng/m^3 (gray).

Table S1. The emission estimates of GEM in Zurich, Switzerland are shown for all observed periods. Additionally, the residual mean squares errors (RMSE) for each period and model fit is shown.

		basic scenario				advanced scenario	
		upper bound		lower bound			
start	days	emissions [g/hour]	RMSE	emissions [g/hour]	RMSE	emissions [g/hour]	RMSE
06/06/2014	4	5.7	0.36	3.8	0.33	8.2	0.37
16/07/2014	5	4.4	0.23	2.5	0.25	5.3	0.32
05/09/2014	4	4.0	0.33	2.4	0.23	3.8	0.24
05/03/2015	6	3.5	0.25	1.7	0.22	1.9	0.28
18/05/2015	5	3.4	0.30	1.1	0.21	2.0	0.22
24/06/2015	14	4.8	0.36	3.0	0.29	5.4	0.35
11/07/2015	13	5.9	0.35	3.8	0.27	4.5	0.33
02/08/2015	5	5.7	0.33	3.7	0.27	3.3	0.40
28/08/2015	4	4.5	0.22	2.7	0.20	3.6	0.27
mean		4.7±0.9		2.8±1		4.9±1.7	
annual [kg/a]		41±8		24±8		43±15	
winter							
07/12/2013		5.1		3.4		-	
10/12/2014		3.6		1.8		-	
08/02/2014		4.6		2.6		-	